Received: 6 January 2020 | Revised: 12 May 2020 | Accepted: 14 June 2020

DOI: 10.1002/2050-7038.12540

WILEY

RESEARCH ARTICLE

Indirect vector controlled of an induction motor using H^∞ current controller for IGBT open circuit fault compensation

Bilal Djamal Eddine Cherif[1] | **Ali Djerioui**[1] | **Samir Zeghlache**[2] | **Sara Seninete**[3] | **Amina Tamer**[4]

[1]Faculty of Technology, Department of Electrical Engineering, University of M'sila, M'sila, Algeria

[2]LASS, Laboratoire d'Analyse des Signaux et Systèmes, Faculty of Technology, Department of Electrical Engineering, University of M'sila, M'sila, Algeria

[3]Laboratoire signaux et systèmes, Electrical Engineering Department, Science and Technology Faculty, Abdelhamid Ibn Badis University, Mostaganem, Algeria

[4]Faculty of Technology, Department of Electrical Engineering, University Ibn-Khaldoun Tiaret, Tiaret, Algeria

Correspondence
Bilal Djamal Eddine Cherif, Faculty of Technology, Department of Electrical Engineering, University of M'sila, M'sila 28000, Algeria.
Email: cherif.bilaldjamaleddine@univ-msila.dz

Peer Review
The peer review history for this article is available at https://publons.com/publon/10.1002/2050-7038.12540.

Summary

The purpose of this paper is to design the robust fault-tolerant control FTC open-circuit fault IGBT's, first of all. The modeling and control of the induction motor in the healthy inverter and in the faulty inverter (open-circuit fault at the IGBT switch) are proposed. Furthermore, the technique for detection and location the open-circuit fault an IGBT based on the Park vector combined with the polar coordinate. In order to ensure the service continuity of the system, two methods of tolerance are developed: the first method, the indirect vector control with H^∞ controller of the induction motor fed by a three-phase inverter based on the fault compensation. The second method, the indirect vector control of the induction motor fed by a three-phase inverter with the redundant leg. Finally, comparative study between the two techniques of tolerance is carried out. The performance of each technique is confirmed by experimental results.

KEYWORDS

H^∞ controller, compensation, detection, FTC, IM, location, Park, reconfiguration, redundant leg, vector control

1 | INTRODUCTION

Currently, the electric drive with AC is considered to be the tool for electromechanical conversion more used in the industrial field. Because this type of drive is justifying by the simplicity of construction, with an optimal cost of maintenance and purchase, like its mechanical robustness. The electric drive made up of the induction motor (IM) associated with static converters at present is used in the industrial applications at a variable speed. The advantages associated with operation at variable speed of the IM can perfectly be carried out only if an appropriate control technique is applied. Indeed, the first control, which was introduced into the industry, was the scalar control. It has very widespread for its simplicity and low cost. It occupied a large part of variable speed applications. The Vector control is a generic

List of Symbols and Abbreviations: IM, induction motor; FTC, fault tolerant control; T_{em}, T_{em2ph}, T_{em3ph}, torque, torque with two phase and torque with three phase; θ_{fk}, fault angle with IGBT; i_{cf}, current vector fault; d, q, two-axis synchronous frame quantities; L_s, L_r, stator and rotor inductances; R_s, R_r, stator and rotor resistances; s, r, stator, rotor; V, I, Φ, voltage, current, and flux, respectively; σ, leakage factor; *, reference value.

term indicating the whole of the controls holding accounts the equations of the controlled system in real-time. This name comes owing to the fact that the final relations are vector, unlike the scalar controls. The relations thus obtained are more complex than those of the scalar control, while it is possible to obtain better performances in transient state.[1]

The industrial constraints of reliability, maintainability, availability, and safety of the equipment are in addition very important. This is why the industrial world is very interesting in the techniques to improve the state of health of this equipment.[2]

Given account the importance of the safety of electrical equipment, it is essential of to conceive of new tolerant architectures, called active fault tolerance or (hardware redundancy) and passive tolerance (control algorithms of the induction machine associated with static converters) who must launch corrective actions and allow the recovery of the configuration of the healthy installation. Or maintain the operation of the system in a degraded mode. In other words, the FTC should avoid the area of danger where the performance is unacceptable.[3-6]

Several researchers were published in the field of material reconfiguration of the static converter (inverter), wherein the authors[7] studied the various PWM inverter fault-tolerant topologies of the variable speed for electric vehicles, which the strategy of detection, insulation, and reconfiguration of the IGBT open circuit fault to operate in degraded mode, some control topologies based on classic vector control such as: 4-wire and 4-leg PWM inverter topologies are investigated. The work of authors[8] consists of new diagnostic techniques based on the Park vectors associated with polar coordinates for the detection and localization of the IGBT open circuit fault as well as the integration of fault-tolerant reconfigurable with redundancy leg inverter in order to enable continuity of service of the wind power system.

Motivated by the above works,[7,8] the concepts of the proposed method is based on a robust vector control system for an induction motor in faulty condition with open-circuit fault at the IGBT switch. The control design is carried out using an appropriate H^{∞} procedure in order to compensate for the fault effects. However, this compensation is performed by the regulation of homopolar current component I_0. Compared with the existing fault tolerant controller designs for induction motor, the main contributions of this work lie in the following:

1. Unlike in References 7 and 8, the proposed control method present a low cost where the redundant leg (multiplication of isolation switches and reconfiguration) is not required. In addition, the proposed control method is characterized by minimal computational time.
2. The fault tolerant control proposed in this work (based H^{∞} control approach) has certain benefit compared to References 9 and 10, which are based on complicate nonlinear control such as sliding mode and backstepping.
3. In Reference 11, authors adopt a complicate fault tolerant control based on observer for faults detection. Unfortunately, this method needs an additional observer, which will augment computational time and high cost, which is not desired for real-time implementation. In this work, H^{∞} control scheme which does not require an observer or diagnostic block.

This paper presents a robust control design to Fault Tolerant Control of IGBT open circuit fault. Firstly, the modeling of IM and its indirect vector control technique applied to both a healthy state and the inverter and an open-circuit fault are proposed. Additionally, a technique based on the Park vectors associated with polar coordinates for the detection and location is detailed. To ensure the continuity of the system's service, both tolerance techniques are developed. The first technique based on indirect vector controlled of an IM using H^{∞} current controller and injecting the zero-sequence current into the control for IGBT open circuit fault compensation and the second technique based on indirect vector controlled of an IM fed by a three-phase voltage inverter with redundancy leg. Finely a rigorous comparative study between the proposed tolerance techniques is carried out. The performance of each technique is validated by experimental results.

2 | INDIRECT VECTOR CONTROL OF INDUCTION MOTOR FED BY HEALTHY AND FAULTY INVERTER

2.1 | Dynamic model of induction motor

The analysis of the operation control of an IM fed by a three-phase voltage inverter is not simply because of the non-linear behavior of these elements. The mathematical model of IM in a rotating field reference is given as follows[11,12]:

- Stator voltage equations[12,13]:

$$\begin{cases} V_{\mathrm{sd}} = R_{\mathrm{s}} i_{\mathrm{sd}} + \dfrac{d}{dt}\varphi_{\mathrm{sd}} - \omega_{\mathrm{s}}\varphi_{\mathrm{sq}} \\ V_{\mathrm{sq}} = R_{\mathrm{s}} i_{\mathrm{sq}} + \dfrac{d}{dt}\varphi_{\mathrm{sq}} + \omega_{\mathrm{s}}\varphi_{\mathrm{sd}} \end{cases} \tag{1}$$

where, φ_{sd}, φ_{sq} are the fluxes, and R_s is the one phase winding resistance

- Rotor voltage equations[12,13]:

$$\begin{cases} 0 = R_{\mathrm{r}} i_{\mathrm{rd}} + \dfrac{d}{dt}\varphi_{\mathrm{rd}} - \omega_{\mathrm{g}}\varphi_{\mathrm{rq}} \\ 0 = R_{\mathrm{r}} i_{\mathrm{rq}} + \dfrac{d}{dt}\varphi_{\mathrm{rq}} + \omega_{\mathrm{g}}\varphi_{\mathrm{rd}} \end{cases} \tag{2}$$

The electromagnetic torque is given as[12,13]:

$$T_{\mathrm{em}} = \frac{3}{2} np \frac{M}{L_{\mathrm{r}}}\left(\varphi_{\mathrm{rd}} i_{\mathrm{sq}} - \varphi_{\mathrm{rq}} i_{\mathrm{sd}}\right) \tag{3}$$

The fundamental equation of mechanics is[12,13]:

$$J\frac{d}{dt}\omega_{\mathrm{r}} + f\omega_{\mathrm{r}} = T_{\mathrm{em}} - T_{\mathrm{r}} \tag{4}$$

The flux-current relationships are[12,13]:

$$\begin{cases} \varphi_{\mathrm{sd}} = L_{\mathrm{s}} i_{\mathrm{sd}} + M i_{\mathrm{rd}} \\ \varphi_{\mathrm{sq}} = L_{\mathrm{s}} i_{\mathrm{sq}} + M i_{\mathrm{rq}} \\ \varphi_{\mathrm{rd}} = M i_{\mathrm{sd}} + L_{\mathrm{r}} i_{\mathrm{rd}} \\ \varphi_{\mathrm{rq}} = M i_{\mathrm{sq}} + L_{\mathrm{r}} i_{\mathrm{rq}} \end{cases} \tag{5}$$

The stator current and rotor-flux model can be given by the following state representation[12,13]:

$$\begin{pmatrix} \frac{d}{dt}\bar{i}_{\mathrm{s}} \\ \frac{d}{dt}\bar{\varphi}_{\mathrm{r}} \end{pmatrix} = \begin{pmatrix} \mathrm{a}_1 & \mathrm{a}_2 \\ \mathrm{a}_3 & \mathrm{a}_4 \end{pmatrix} \begin{pmatrix} \bar{i}_{\mathrm{s}} \\ \bar{\varphi}_{\mathrm{r}} \end{pmatrix} + \begin{pmatrix} 1 \\ 0 \end{pmatrix} \frac{\bar{V}_{\mathrm{s}}}{\sigma L_{\mathrm{s}}} \tag{6}$$

Where,

$$a_1 = \left(R_{\mathrm{s}} + m_{\mathrm{r}}\frac{M}{T_{\mathrm{r}}}\right)\frac{1}{\sigma T_{\mathrm{r}}}, a_2 = -\frac{m_{\mathrm{r}}}{\sigma L_{\mathrm{s}}}\left(J\omega - \frac{1}{T_{\mathrm{r}}}\right), a_3 = \frac{M}{T_{\mathrm{r}}}, a_4 = J\omega - \frac{1}{T_{\mathrm{r}}}$$

2.2 | Indirect rotor field oriented control with a healthy inverter

In order to establish a vector control we recall here its modeling in an arbitrary rotating (d, q) Park reference frame, so that the rotor flux is aligned with the axis (d) makes it possible to obtain a torque expression in which two orthogonal currents (i_{ds}, i_{qs}) intervene; the first flux generator and the other torque generator, Figure 1.[14]

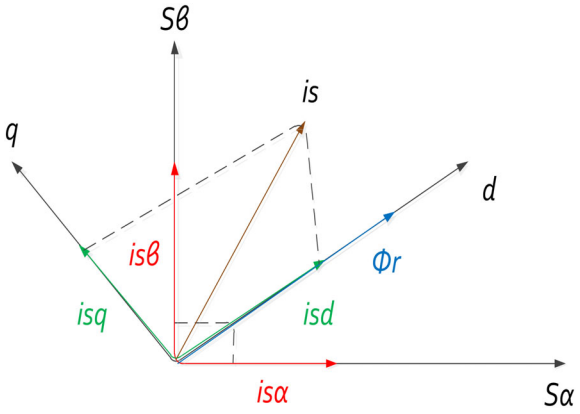

FIGURE 1 Vector diagram of the rotor flux orientation strategy

Thus, the rotor flux orientation concept is allows giving[15,16]:

$$\begin{cases} \varphi_{rq} = 0 \\ \varphi_{rd} = \varphi_r \end{cases} \tag{7}$$

Under these conditions, the voltage equations of the rotor are the following[15,16]:

$$\begin{cases} 0 = R_r i_{rd} + \dfrac{d}{dt}\varphi_{rd} \\ 0 = R_r i_{rq} + \omega_r \varphi_{rd} \end{cases} \tag{8}$$

The electromagnetic torque equation becomes[15,16]:

$$T_{em} = \frac{3}{2} np \frac{M}{L_r} \varphi_{rd} i_{sq} \tag{9}$$

The estimated rotor flux gives[15,16]:

$$\frac{d}{dt}\hat{\varphi_r} = -\frac{1}{T_r}(\hat{\varphi_r} - M i_{sd}) \tag{10}$$

The sliding speed estimation given by[15,16]:

$$\hat{\omega_g} = \frac{M}{T_r} \frac{i_{sq}}{\hat{\varphi_r}} \tag{11}$$

The Park current references $\left(i_{ds}^*, i_{qs}^*\right)$ can be given by[15,16]:

$$\begin{cases} i_{ds}^* = \dfrac{2}{3} i_{as}^* - \dfrac{1}{3} i_{bs}^* - \dfrac{1}{3} i_{cs}^* \\ i_{qs}^* = \dfrac{1}{\sqrt{3}}\left(i_{bs}^* - i_{cs}^*\right) \end{cases} \tag{12}$$

2.3 | Vector control by rotor flux orientation with a faulty inverter

In the case of an upper IGBT open-circuit fault of phase A, the current of phase A equals zero, howsoever $i_{as}^{*}=0$. The Park current references $\left(i_{ds}^{*},i_{qs}^{*}\right)$ can be given by[7,17,18]:

$$\begin{cases} i_{ds}^{*}=-\dfrac{1}{3}i_{bs}^{*}-\dfrac{1}{3}i_{cs}^{*} \\ i_{qs}^{*}=\dfrac{1}{\sqrt{3}}\left(i_{bs}^{*}-i_{cs}^{*}\right) \end{cases} \tag{13}$$

The torque in the case of two-phase control is expressed by the relation[7,17,18]:

$$T_{em2ph}=\frac{2}{3}T_{em3ph}=\frac{PM}{L_r}\varphi_{rd}I_{sq} \tag{14}$$

The ratio between the electromagnetic torque of healthy case and open-circuit fault case is expressed by[7,17,18]:

$$\frac{T_{em2ph}}{T_{em3ph}}\approx 0.666 \tag{15}$$

3 | PRESENTATION OF THE TEST RIG

In order to validate the analysis and design, Figure 2 depicts the laboratory setup for investigating the proposed methods for three-phase IM (Appendix A) though employing DSPACE 1104 for acquisition and processing. According to the affected inverter part; in our case, open-circuit fault IGBT's switches (K_1, K_2, K_3, K_4, K_5, and K_6) each fault has a characteristic frequency which is reflected in the stator current signal at well-determined frequencies. The instruments and equipment used in the experimental tests: Three-phase IM (triangle coupling, 50 Hz, 04 poles, 3Kw), Inverter (a three-phase two-level). The measurement chain includes three FLUCK i30s hall effect current sensor (AC/DC current clamp), three Tektronix P5200 voltage sensors, torque sensor, speed sensor and a DSPACE 1104. The tested IM is coupled to a 2.4 Kw direct current generator forming the test bench.[19]

The acquisitions are carried out under steady state conditions with a sampling frequency $F_e = 10\ 000$ Hz and with an acquisition time $t_{acq} = 20$ seconds and with frequency resolution $\Delta f = 0.05$ Hz and the rated load operation with a rated current of 7A and an estimated torque of 20 Nm.

The basic scheme as shown in Figure 3 illustrates the indirect vector control of induction motor fed by two-level inverter.

Figure 4 depicts the experimental results of the vector control applied to a healthy and faulty inverter.

In the case of healthy inverter, shows the behavior of IM fed by both a healthy inverter for a speed reference during a load start. Note that for the case of the healthy inverter, the shape of the speed follows perfectly its reference without any overshoot which is reached very quickly. It can also be noticed small oscillations of the instantaneous torque during startup but for a very short time. It is clear that the performance of the speed regulation loop is satisfactory and its rise time is acceptable and even the rejection of the disturbance is ensured.

In the case of faulty inverter, shows the behavior of the induction motor fed by both a faulty inverter for a speed reference during a load start. In the abnormal regime, the electrical quantities (the stator currents) are compared to the normal regime considered as the reference. Due to the sudden change in the current of phase A, characterized by the disappearance of the positive alternation at the instant of the K_1 IGBT switch open-circuit fault occurrence, the phase current connected to the faulty arm is no longer controlled as it is only negative or zero. Under these conditions the current of the other two healthy phases (zero sum) take instantaneously high values. Furthermore, it should also be noted that the IGBT fault influences the mechanical behavior of the motor. This influence is characterized by a fall in the speed value, as well as a variation (oscillations) of the electromagnetic torque resulting in a degraded operation of the motor.

(A)

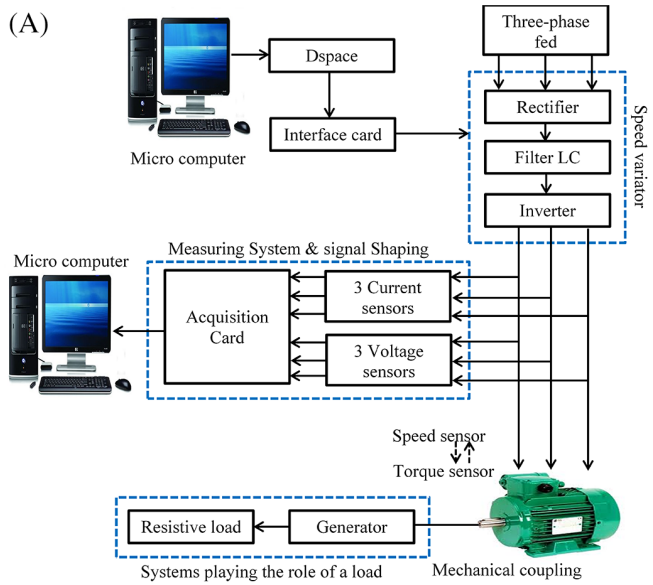

FIGURE 2 Experimental test-rig (A)

(B)

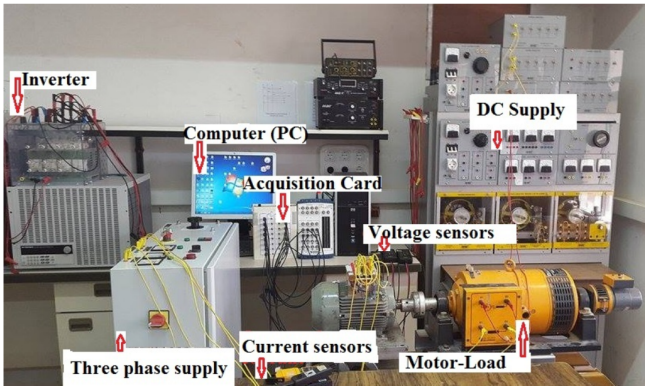

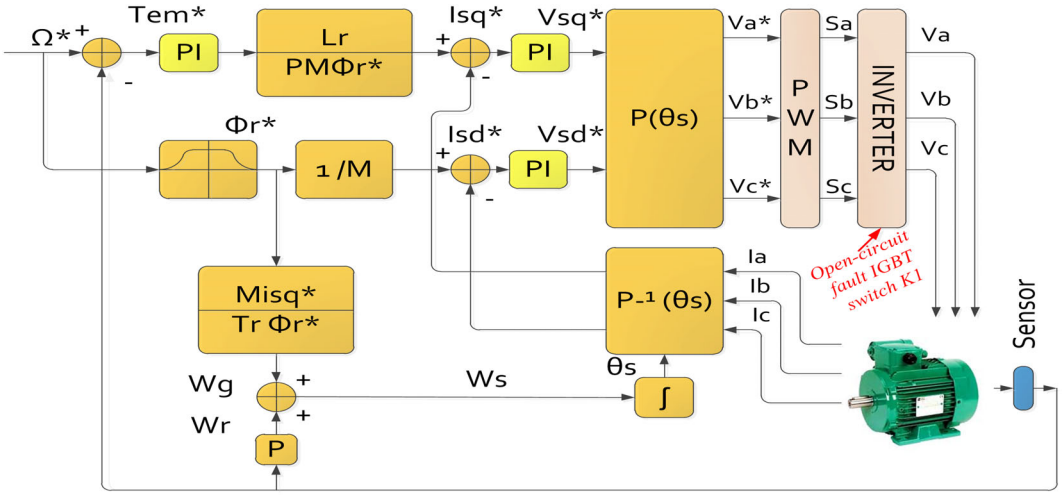

FIGURE 3 Basic scheme of IFOC for IM fed by two-level inverter

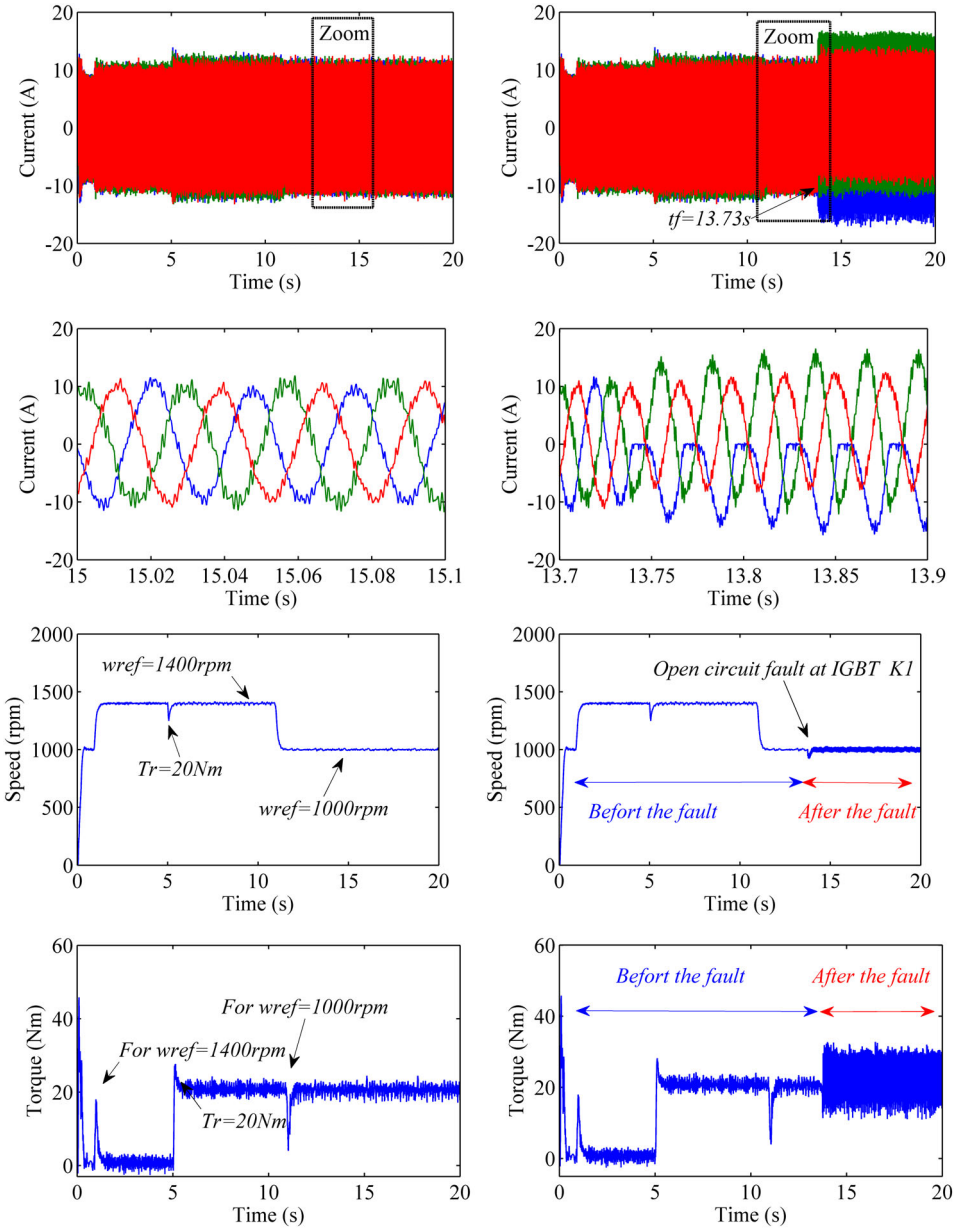

FIGURE 4 Experimental results of IFOC for a healthy and faulty inverter (case of healthy inverter and case of open-circuit fault

4 | DETECTION AND LOCATION THE OPEN-CIRCUIT FAULT EACH IGBT SWITCH

The detection and location technique based on the Park approach combined with polar coordinates.[20]

The fault angle is calculated from Equations 16-18 as follows.[20]

$$\theta_{fk} = \sum_{i=0}^{N} \frac{\pi r^2 \rho}{360} \tag{16}$$

The radius of this trajectory can be calculated from the following equation[20]:

$$r = \sqrt{(i_{ds})^2 + (i_{qs})^2} \tag{17}$$

$$\rho = \rho_{max} - \rho_{min} \tag{18}$$

The (d, q) currents at the center of the trajectory i_{dc} and i_{qc} can be computed using the maximum and minimum of the currents vectors as follows[20]:

$$\begin{cases} i_{dsc} = \frac{1}{2}(i_{dsmax} + i_{dsmin}) \\ i_{qsc} = \frac{1}{2}(i_{qsmax} + i_{qsmin}) \end{cases} \tag{19}$$

The fault current vector of each IGBT, expressed by the following equation[20]:

$$i_{cf} = i_{dsc} + j i_{qsc} \tag{20}$$

Figure 5 shows the experimental results of three-phase stator current fault vectors in the healthy case and open-circuit fault case of each IGBT.

According to Figure 5 it is possible to calculate the intervals of the faulty angles of each leg, the intervals of the faulty angles of each IGBT and the exact faulty angles of each IGBT.

The information of each IGBT for the healthy and faulty inverter cases are summarized in Table 1.

Figure 6 shows the detection time by Park approach combined with polar coordinates can be defined as shown in the figure below.

The time taken by the Park approach combined with polar coordinates is 0.005 second, which is enough to ensure the continuity of service of the production system.

5 | CONTROL STRATEGY CONCEPT RECONFIGURATION WITH A FAULTY INVERTER

This section presents two fault-tolerant control strategies:

- Indirect vector controlled concept of an IM fed by a three-phase inverter based on the tolerant control with IGBT open circuit fault compensation, proposed method.
- Indirect vector controlled concept of an IM fed by a three-phase voltage inverter with redundancy leg.

5.1 | Indirect vector controlled concept of an IM using H^∞ current controller of an IM fed by a three-phase voltage inverter based on the tolerant control with IGBT open circuit fault compensation

The fault tolerant control proposed in this section is illustrated by the synoptic diagram (Figure 7).

- The H^∞ control design

The H^∞ mixed standard sensitivity current controller is employed in this part .For mixed sensitivity optimization of H^∞ control theory, the weighting filters $W_1(s)$, $W_2(s)$, and $W_3(s)$ are used to guide the H^∞ to generate a controller that meets the required specifications (ant disturbance, and robustness). For the IGBT open-circuit fault inverter. A plant model for the controller synthesis is shown in Figure 8.[21,22]

Figure 9 shows the standard configuration H^∞.[23,24]

The associated general control configuration is given as[25,26]:

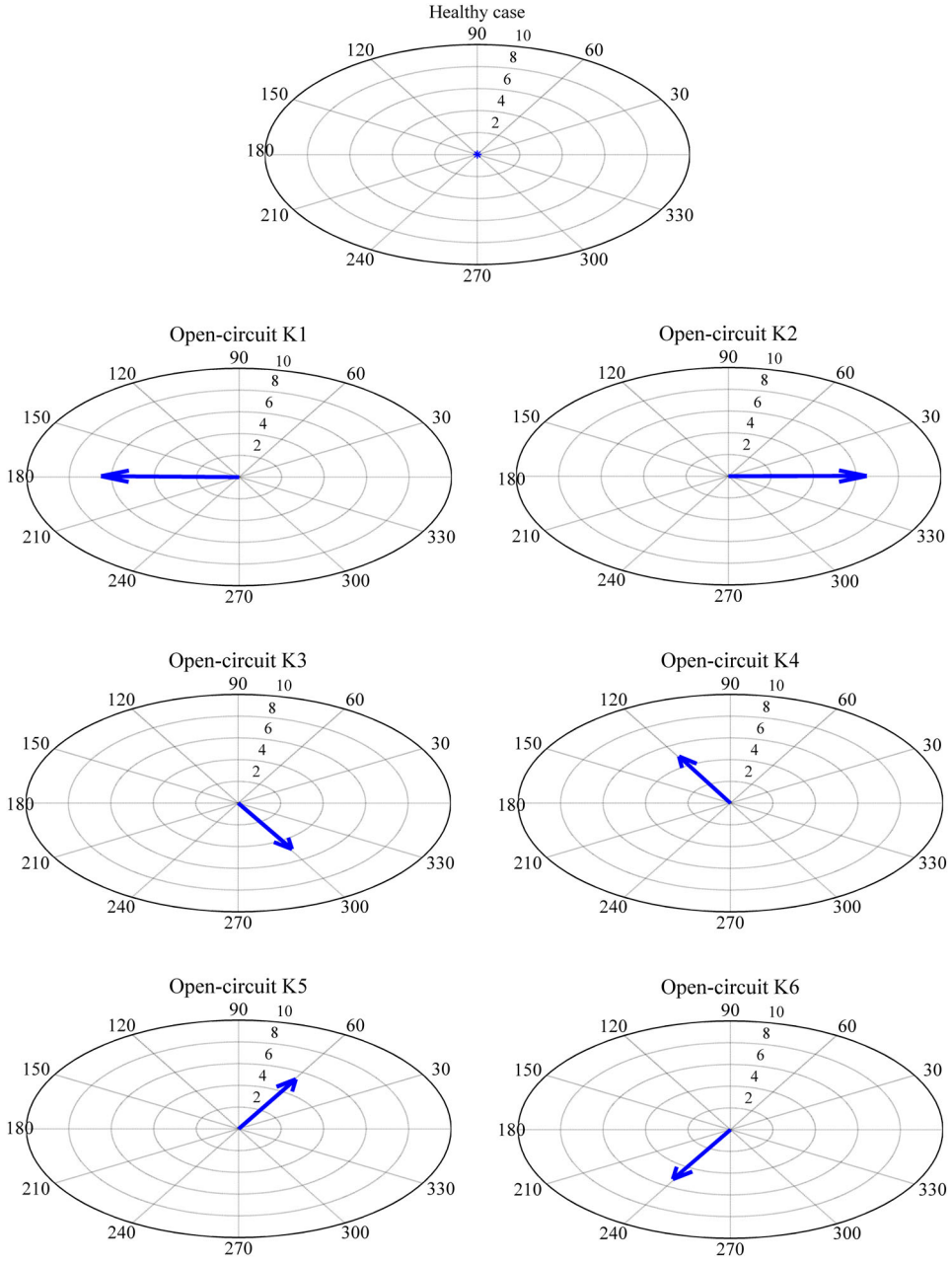

FIGURE 5 Fault vectors of the healthy case and open-circuit faulty case of each IGBT

$$\begin{bmatrix} y_1 \\ y_2 \\ y_3 \\ e \end{bmatrix} = \begin{bmatrix} W_1 & -W_1 G \\ 0 & -W_2 \\ 0 & -W_3 G \\ \mathrm{I} & -G \end{bmatrix} \begin{bmatrix} I^* \\ u \end{bmatrix} \tag{21}$$

We can write a mixed sensitivity problem as[25,26]:

$$P = \begin{bmatrix} W_1 S \\ W_2 K S \\ W_3 T \end{bmatrix} \tag{22}$$

In case of mixed sensitivity problem our objective is to find a rational function controller $K(s)$ and to make the closed loop system stable satisfying the following expression[25,26]:

TABLE 1 Shows the intervals of these angles and the fault current vectors of each IGBT

IGBT	The intervals of the faulty angles of each leg		The intervals of the faulty angles of each IGBT	Fault current vector of each IGBT
Healthy case	[0°, 360°]		[0°, 360°]	$0.003152 \angle 2^{\circ}$
Open-circuit K_1	Leg A	[−90°, 90°]	[150°, 210°]	$5.75 \angle 176.8882^{\circ}$
Open-circuit K_2			[330°, 30°]	$5.3462 \angle 359.6198^{\circ}$
Open-circuit K_3	Leg B	[−150°, 30°]	[270°, 330°]	$3.4184 \angle 292.7804^{\circ}$
Open-circuit K_4			[90°, 150°]	$3.7621 \angle 111.1316^{\circ}$
Open-circuit K_5	Leg C	[−30°, 150°]	[30°, 90°]	$3.7279 \angle 69.5234^{\circ}$
Open-circuit K_6			[210°, 270°]	$3.6415 \angle 244.5908^{\circ}$

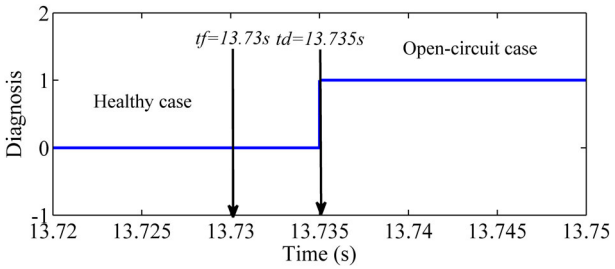

FIGURE 6 Chronology of operation in healthy case, during the fault and the operation after the open circuit fault of IGBT K1

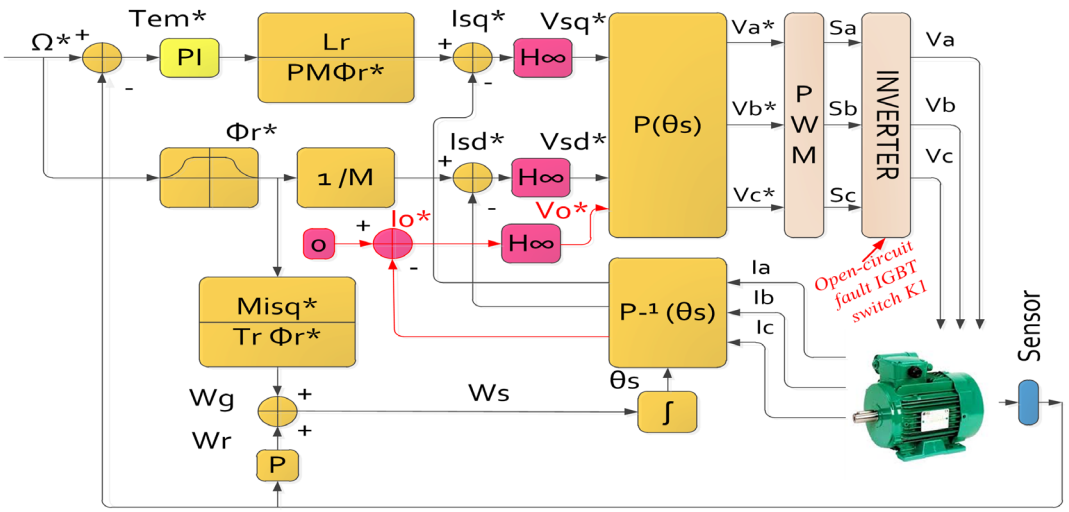

FIGURE 7 Synoptic diagram of FTC proposed method

$$\text{Min}\|\text{P}\| = \text{Min}\begin{bmatrix} W_1 S \\ W_2 K S \\ W_3 T \end{bmatrix} = \gamma \tag{23}$$

where, P is the transfer function from I^* *to* y *i. e.*

The corresponding H_∞ suboptimal control problem is therefore to find a controller $K(s)$ such that

$$\left|T_{yI^*}\right| \leq \gamma \tag{24}$$

FIGURE 8 Plant model for the controller synthesis[22,23]

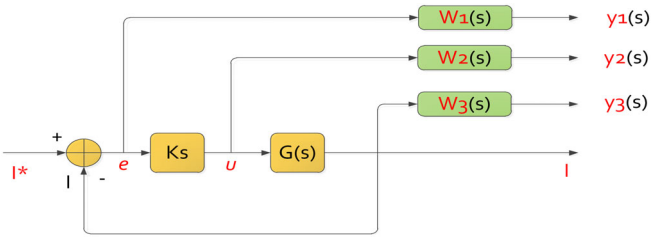

FIGURE 9 Standard configurations H^{∞}

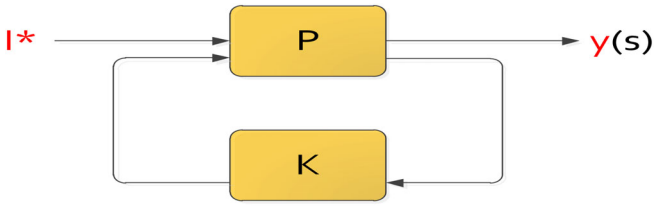

where, $\left|T_{yI^*}\right| = P$ is the cost function

The weighting filters are chosen as:

$$W_1 = \frac{0.5(s+10)}{(s+0.15)} \tag{25}$$

$$W_2 = 0 \tag{26}$$

$$W_3 = \frac{20(s+10))}{(s+400)} \tag{27}$$

The full-order H^{∞} controller is given by:

$$K(s) = \frac{0.1s^2 + 37.3s + 2689}{0.0037s^2 + 6.0941s + 0.9129} \tag{28}$$

Figure 10 shows that S and T achieve the desired loop shape, where S is large inside the control bandwidth and γ is small outside the control bandwidth. To see how mixed-sensitivity loop shaping achieves the goals of classic loop shaping, compare the open-loop response L to the weighting filters. $L \sim W_1$ where W_1 is large, and $L \sim 1/W_3$ where W_3 is large.

5.2 | Indirect vectors controlled concept of an IM fed by a three-phase voltage inverter with redundancy leg

The fault tolerant topology in Figure 11 includes a redundant leg connected using bidirectional voltage and current switches (triacs) to the converter. This redundant leg is constituted of two power switches K and K′ and replaces one of the other converter legs when a fault occurs on a switch of that leg.[27,28]

The equations of the reference current (i^*_{as},i^*_{bs},i^*_{cs},i^*_{rl}):

- In the healthy case the currents are given as follows[27,28]:

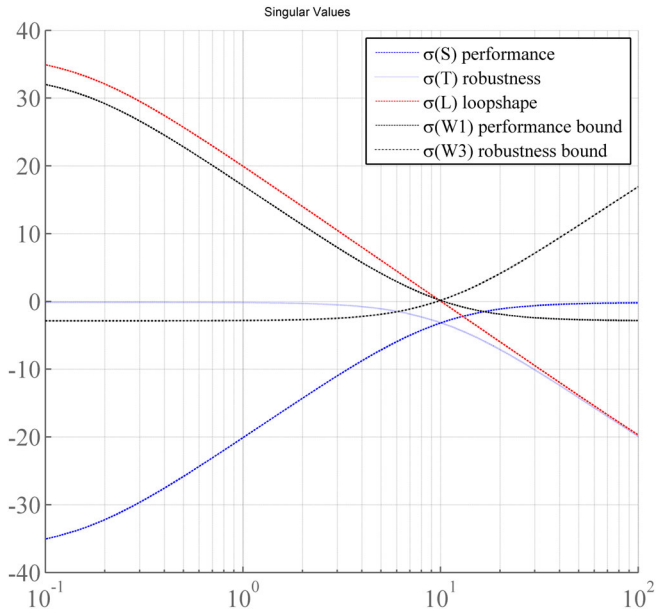

FIGURE 10 Performance bounds for H^{∞} control

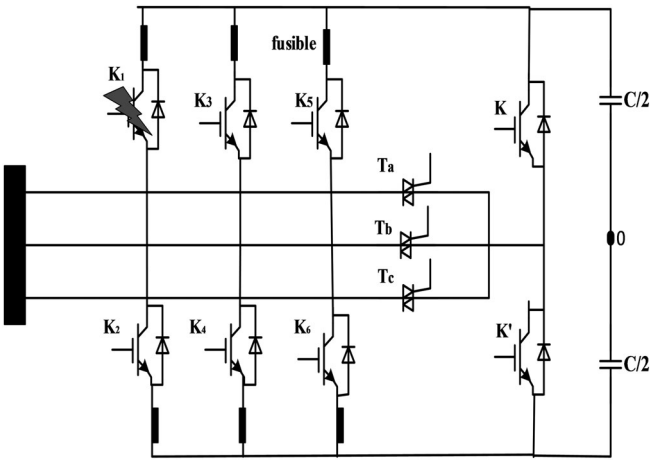

FIGURE 11 Fault tolerant of the two-level inverter topology

$$\begin{cases} i_{as}^{*} = i_{qs}^{*}\cos(\varphi) + i_{ds}^{*}\sin(\varphi) \\ i_{bs}^{*} = i_{qs}^{*}\cos\left(\varphi - \frac{2\pi}{3}\right) + i_{ds}^{*}\sin\left(\varphi - \frac{2\pi}{3}\right) \\ i_{cs}^{*} = i_{qs}^{*}\cos\left(\varphi - \frac{4\pi}{3}\right) + i_{ds}^{*}\sin\left(\varphi - \frac{4\pi}{3}\right) \\ i_{rl}^{*} = 0 \end{cases} \tag{29}$$

- In the case of open-circuit fault the currents are given as follows[27,28]:

$$\begin{cases} i_{as}^{*} = 0 \\ i_{bs}^{*} = i_{qs}^{*}\cos\left(\varphi - \frac{2\pi}{3}\right) + i_{ds}^{*}\sin\left(\varphi - \frac{2\pi}{3}\right) \\ i_{cs}^{*} = i_{qs}^{*}\cos\left(\varphi - \frac{4\pi}{3}\right) + i_{ds}^{*}\sin\left(\varphi - \frac{4\pi}{3}\right) \\ i_{rl}^{*} = i_{qs}^{*}\cos(\varphi) + i_{ds}^{*}\sin(\varphi) \end{cases} \tag{30}$$

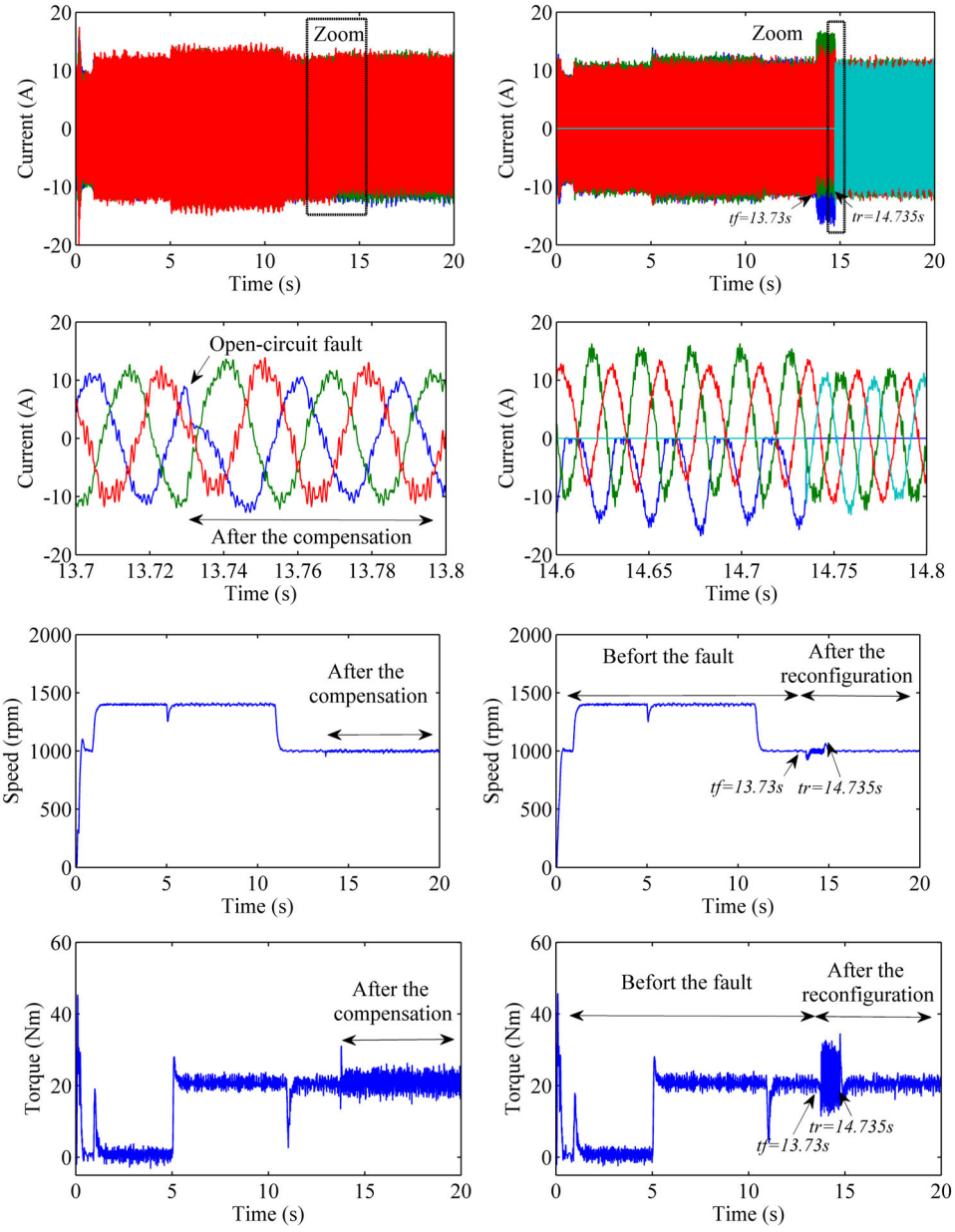

FIGURE 12 FTC strategies with H$^{\infty}$ controller and redundant leg (FTC strategies with H_controller and FTC strategies with redundant leg)

Figure 12 shows the results of the FTC strategy in the case of IGBT open circuit fault (switch K_1).

FTC strategies with H$^{\infty}$ H$^{\infty}$ controller presents the responses of this control strategy for K_1 open-circuit fault in leg A at time $t = 13.73$ seconds. It is noted that the regulator eliminates the K_1 open circuit fault effect in a very rapid time how giving acceptable performance, which we can note that this method assured the fault compensation.

FTC strategies with redundancy leg: presents the responses of this control strategy for K_1 open-circuit fault in leg A at time $t = 13.73$ seconds. It can be seen in this control strategy that the performance of the variable speed drive after a fault is maintained the same as in the healthy case. This observation is justified by the command signals of redundancy leg are the same as those of the faulty leg.

TABLE 2 Comparative study

Proposed method	Redundancy leg		
Implantation			
Based on robust algorithms	The command signals of redundancy leg are the same as those of the faulty leg		
Simple and quick Implantation	Easy and quick Implantation		
Hardware			
No hardware	Multiplication of isolation switches and reconfiguration		
No hardware	An increasing number of sensors and close-up card		
Time (s)			
Reconfiguration time			
0	1.005		
Compensation time			
0.005	0		
THD signal quality (%)			
Before the fault	After the fault	Before the fault	After the fault
3.88	7.45	3.88	3.895
Complexity			
Medium	Low		

6 | COMPARATIVE STUDY BETWEEN THE TWO METHODS

The aim of this comparison between the two methods previously proposed is for evaluating each one in terms of performance that is, capacity and speed of fault tolerance and also in the terms of materials used that is, the number of sensors and switches, this below illustrated comparative study in the Table 2.

This table clearly shows that the proposed method, indirect vector controlled of an IM using H^{∞} current controller with the faster regulator in terms of compensation time and reconfiguration system (0.005 second) compared to the redundancy leg method (1.005 seconds). The proposed method does not require an increase in the number of switches, the number of sensors and close-up card, also has an advantage over indirect vector control the redundancy leg method in terms of cost. Unfortunately, the proposed method also presents a suitably related to the quality of the signal (THD) after the compensation and the reconfiguration of the system. The proposed method takes a value of (THD = 7.45% <10%) and the redundancy leg method takes a value of (THD = 3.895% <10%).

7 | CONCLUSION

The current paper aims to study, develop and proposal for an IGBT open-circuit fault compensation of PWM inverter fed induction motor, two techniques of tolerance were proposed and their performances were discussed. One method was based on indirect vector controlled of an IM using H^{∞} current controller and the other was based on an indirect vector controlled of an IM fed by a three-phase voltage inverter with redundancy leg. A detailed comparative study is also carried out between these two techniques to assess each technique in terms of performance and in terms of equipment. To validate these last, an experimental test-rig has been developed which consists of a two-level voltage inverter controlled by a DSPACE-1104 card to generate the indirect vector control of IM. Experimental results prove the effectiveness of compensation and reconfiguration of each technique.

ORCID

Bilal Djamal Eddine Cherif https://orcid.org/0000-0001-7703-2295

REFERENCES

1. Bilal Djamal Eddine CH, Azeddine BA, Mokhtar B, Amina T. Neural network based fault diagnosis of three phase inverter fed vector control induction motor. *J Per Poly Electr Eng Comput Sci*. 2019;63(4):295-305.
2. Orlowska-Kowalska T, Sobanski P. Simple diagnostic technique of a single IGBT open-circuit faults for a SVM-VSI vector controlled induction motor drive. *Bull Pol Acad Tech*. 2015;63(1):281-288.
3. Afef F. Fault diagnosis and fault tolerant control design for aerospace systems: A bibliographical review. In : 2014 American Control Conference. IEEE, 2014. p. 1286–1291.
4. Blanke M, Kinnaert M, Lunze J, Staroswiecki M. *Diagnosis and Fault-Tolerant Control*. Berlin: Springer; 2006.
5. Maamouri R, Trabelsi M, Boussak M, M'Sahli F. Fault diagnosis and fault tolerant control of a three-phase VSI supplying sensorless speed controlled induction motor drive. *Electr Power Comp Syst*. 2018;46(19):2159-2173.
6. Sahraoui K, Gaoui B. Fast detection control for fault-tolerant converter back-to-back with redundancy leg supplying an induction motor drives. *Int J Dig Sig Smart Syst*. 2018;2(1):15-35.
7. Tabbache B, Benbouzid M, Kheloui A, Bourgeot J, Mamoune A. An improved fault-tolerant control scheme for PWM inverter-fed induction motor-based EVs. *ISA Trans*. 2013;52(6):862-869.
8. Omar Fethi B, Azzeddine BA, Kahla S. Contribution à la reconfiguration d'onduleur à tolérance de panne appliquée au parc éolien connecté au réseau électrique. *Rev Roum Sci Techni-électrotechn et énerg*. 2019;64(2):143-148.
9. Djeghali N, Ghanes M, Djennoune S, Barbot JP. Sensor less Ault tolerant control for induction motors. *Int J Cont Autom Syst*. 2013;11 (3):563-576.
10. Fekih A. Effective fault tolerant control design for nonlinear systems: application to a class of motor control system. *IET Cont Theo Appl*. 2008;2(9):762-772.
11. Rebah M, Mohamed T, Mohamed B, Faouzi M. Mixed model based and signal based approach for open-switches fault diagnosis in sensorless speed vector controlled induction motor drive using sliding mode observer. *IET Power Electron*. 2019;12(5):1149-1159.
12. El-Barbar ZM, Azazi HZ. Experimental investigation of a speed-sensor-less IM drive system under inverter fault-tolerant control. *IEEJ Trans Electr Electron Eng*. 2016;11(S1):S155-S163.
13. Dorjsuren Y, Tumenbayar L, Tsevegmid J. Three-axis dynamic modeling of induction motor. *Int J Math Mod Appl Sci*. 2015;9(1): 527-536.
14. Jianghan Z, Jin Z, Dehong Z, Chengguang H. High-performance fault diagnosis in PWM voltage-source inverters for vector controlled induction motor drives. *IEEE Trans Power Electron*. 2014;29(11):6087-6099.
15. Najmeh R, Kamyar M, Cossar C. Modelling and analysis of indirect field-oriented control of SVPWM-driven induction motor drive based on a voltage source inverter. Conference: IEEE CCECE 2018; At Canada.
16. Layadi N, Zeghlache S, Benslimane T, Berrabah F. Comparative analysis between the rotor flux oriented control and Backstepping control of a double star induction machine (DSIM) under open-phase fault. *AMSE J AMSE IIETA*. 2017;72(4):292-311.
17. Zhang W, Xu D, Enjeti PN, Li H, Hawke JT, Krishnamoorthy HS. Survey on fault-tolerant techniques for power electronic converters. *IEEE Trans Power Electron*. 2014;29(12):6319-6633.
18. Jannati, M, Idris, NRN, Salam, Z. A new method for modeling and vector control of unbalanced induction motors. IEEE Energy Conversion Congress and Exposition (ECCE); 2012; Raleigh, NC, USA. pp. 3625–3632.
19. Cherif BDE, Bendiabdellah A. Detection of two-level inverter open-circuit fault using a combined DWT-NN approach. *J Contr Sci Eng*. 2018;2018:1976836.
20. Shi T, He Y, Deng F, Tong J, Wang T, Shi L. Online diagnostic method of open-switch faults in PWM voltage source rectifier based on instantaneous AC current distortion. *IET Electr Power Appl*. 2018;12(3):447-454.
21. Jiang Y, Hongsheng L, Bin F, Xingyan X. H∞ mixed sensitivity control for a three-port converter. *Energies*. 2019;12(12):2231.
22. Saihi L, Berbaoui B, Glaoui H, Djilali L, Abdeldjalil S. Robust sliding mode H∞ controller of DFIG based on variable speed wind energy conversion system. *Period Polytech Electr Eng Comput Sci*. 2020;64(1):53-63.
23. Mitov A, Slavov T, Kralev J, Angelov I. H-Infinity Control of an Electrohydraulic Power Steering System. 41st International Conference on Telecommunications and Signal Processing–TSP-2018, IEEE Conference; 2018; Athens, Greece. ISBN: 978–1–5386-4696-0.
24. Wang Y, Wu Q, Gong W, Gryning MPS. H∞ robust current control for DFIG-based wind turbine subject to grid voltage distortions. *IEEE Trans Sustain Energy*. 2017;8(2):816-825.
25. Carolina L, Anders R. Optimal H infinity state feedback for systems with symmetric and Hurwitz state matrix. In Proceedings of American Control Conference; July 2016; Boston.
26. Chayaopas N, Assawinchaichote W. H∞ fuzzy integral power control for DFIG wind energy system. *Int J Electr Comput Eng*. 2017;11(5): 547-553.
27. Kwak S. Four-leg-based fault-tolerant matrix converter schemes based on switching function and space vector methods. *IEEE Trans Ind Electron*. 2012;59(1):235-243.
28. Errabelli R, Mutschler P. Fault-tolerant voltage source inverter for permanent magnet drives. *IEEE Trans Power Electron*. 2012;27(2): 500-508.

How to cite this article: Cherif BDE, Djerioui A, Zeghlache S, Seninete S, Tamer A. Indirect vector controlled of an induction motor using H^{∞} current controller for IGBT open circuit fault compensation. *Int Trans Electr Energ Syst*. 2020;e12540. https://doi.org/10.1002/2050-7038.12540

APPENDIX A: PARAMETERS INDUCTION MOTOR

Rated power: 3KW
Supply frequency: 50 Hz
Rated voltage: 380 V
Rated current: 7A
Rotor speed: 1440 rev/min
Number of rotor bars: 28
Number of stator slots: 36
Power factor: 0.83
Number of pair of poles: 2